Composites Part B 157 (2019) 283–288

Contents lists available at ScienceDirect

Composites Part B

journal homepage: www.elsevier.com/locate/compositesb

Simplification of finite element modeling for plates structures with constrained layer damping by using single-layer equivalent material properties

Jing Zhao[a,b], Pak Kin Wong[a,*], Xinbo Ma[a,b], Zhengchao Xie[c,a,**], Jun Xu[d,e], V.A. Cristino[a]

[a] Department of Electromechanical Engineering, University of Macau, Taipa, Macao
[b] School of Electromechanical Engineering, Guangdong University of Technology, Guangzhou, 510076, PR China
[c] School of Mechanical and Automotive Engineering, South China University of Technology, Guangzhou, 510076, PR China
[d] Department of Mechanical Engineering and Engineering Science, The University of North Carolina at Charlotte, Charlotte, NC, 28223, USA
[e] North Carolina Motorsports and Automotive Research Center, The University of North Carolina at Charlotte, Charlotte, NC, 28223, USA

ARTICLE INFO

Keywords:
Finite element modeling
Simplified single-layer equivalent modeling
Equivalent material properties
Constrained layer damping plate

ABSTRACT

As an effective approach of suppressing vibrations, the constrained layer damping (CLD) has drawn wide attention from the automotive and aerospace industries. However, most of the existing investigations focus on the beam structures with CLD and few studies have been done on the plate structures with CLD. Considering the practical applications, this work studies the finite element (FE) modeling of plate structures with CLD by considering the shear and extension strains in all of three layers. To reduce the computational cost and ensure the accuracy, a simplified single-layer equivalent method is originally proposed to model the plate structure with CLD based on the equivalent material properties. In this method, the equivalent material properties are obtained by defining a new equation which includes the equivalent bending stiffness. By nonlinear regression of these responses at resonance frequencies, the equivalent bending stiffness can be obtained, and the plate structure with CLD can be regarded as a regular single-layer plate for modeling. The simulation result shows that the proposed simplified single-layer equivalent method using single-layer equivalent material properties is efficient and accurate for modeling plate structures with CLD.

1. Introduction

In recent decades, the vibration control has been an active topic with the effective solution of constrained layer damping (CLD) in both automotive and aerospace industries [1–8]. The CLD structure consists of three layers. The constraining layer and base layer with the elastic material sandwich a damping layer which is made up of viscoelastic material [9–11]. With the relative motion of the constraining layer and base layer, a deformation of the damping layer is generated to consume a portion of the strain energy, thus achieving the vibration damping [12–14]. Considering the complexity and geometry properties of the material, it is a challenge to model the CLD structure.

Recently, various researches have been done on the study of CLD structures. Panda et al. [15] studied the performance of the active CLD for beam structures. Özer [16] conducted the modeling and controlling of a fully dynamic three-layer cantilever beam with active constrained layer by using the vibrational approach. Hujare and Sahasrabudhe [17] investigated the damping performance of different viscoelastic material for beams experimentally using CLD treatment. Even though these research facilitates the development of CLD structures, existing studies mainly focus on beam structures, and only few attention has been paid on the modeling of plate structures. Considering the widespread application of plate structures in various fields of engineering, this work tries to investigate the modeling of plate structures with CLD.

As for the numerical analysis of the structural vibrations, the finite element modeling is a good method which has been extensively and efficiently applied to investigate the vibrational behavior of structures including the viscoelastic material [1,10,18,19]. When modeling this plate structure using finite element method, the plate is meshed into many finite elements. Meanwhile, the degrees of freedom should be well defined with fully consideration of the shear, compression and extensional damping. With three layers, the FE modeling of plate structures with CLD is very complicated due to the involved overwhelming degrees of freedom, especially for the plate structure with a

* Corresponding author. Department of Electromechanical Engineering, University of Macau, Macao.
** Corresponding author. School of Mechanical and Automotive Engineering, South China University of Technology, Guangzhou, 510006, PR China.
E-mail addresses: fstpkw@umac.mo (P.K. Wong), zxie@scut.edu.cn (Z. Xie).

https://doi.org/10.1016/j.compositesb.2018.09.010
Received 12 August 2018; Received in revised form 2 September 2018; Accepted 5 September 2018
Available online 06 September 2018
1359-8368/

quite thin damping layer. As a result, the FE modeling of plate structures with CLD cannot be well applied in engineering design. However, the precise results might not be obtained when reducing the degrees of freedom and meshed elements. To solve this problem, a simplified method should be developed to reduce the computational cost and ensure high accuracy. In Ref. [20], a simplified FE modeling for beam structures with CLD is presented by using single-layer equivalent finite element method. The equivalent material properties are calculated and then a regular beam is constructed. Considering the simplicity and accuracy, this work also attempts to develop a simplified equivalent single-layer modeling for plate structures with CLD using single-layer equivalent material properties.

In this research, a simplified single-layer equivalent method is proposed to model the plate structure with CLD based on the equivalent material properties for achieving low computational cost and high accuracy. The rest of this paper is organized as follows. Section 2 presents the FE modeling for the plate structure with CLD. Subsequently, the simplified single-layer equivalent model of the plate structure with CLD is described in Section 3. Finally, conclusions are given in Section 4.

2. Finite element modeling of plate structures with CLD

This section presents the FE modeling of the plate structure with CLD. First, some assumptions are made, and then the modeling process is presented. Finally, the model developed is evaluated by simulation results.

2.1. Assumptions

Before introducing the finite element modeling for plate structures with CLD, the following assumptions are made [21–24]:

(1) The transverse displacement of each layer is identical at the same position;
(2) The longitudinal displacement caused by the shear or extension strain is linearly distributed across the thickness of each layer;
(3) The slip does not occur among the layers.

2.2. Finite element modeling process

The plate structure is shown in Fig. 1. Layer 1, layer 2 and layer 3 are the constraining layer, damping layer and base layer, respectively. The transverse displacement is along with the z-axis, while the longitudinal displacements caused by the shear and extension strain are along with the x-axis and y-axis, respectively.

When modeling this plate structure using finite element method, the plate is meshed into many finite elements first. When meshing these

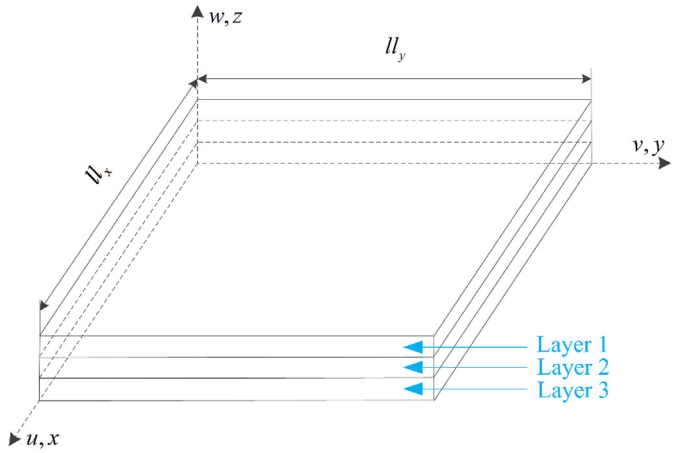

Fig. 1. Plate structure with CLD.

finite elements, n_x and n_y nodes are used in the directions of the x-axis and y-axis, respectively. As a result, $(n_x - 1) \times (n_y - 1)$ finite elements can be obtained for the plate structure with CLD. One finite element in the plate structure with CLD is shown in Fig. 2 based on the Zapfe's element in dealing with the beam structure [25]. In this plate finite element, both the shear strain and extension strain are considered with a high accuracy. To fully characterize the shear strain and extension strain and clearly represent the transverse displacement at each location of the plate, 25 degrees of freedom (DOFs) are defined for the plate finite element with one layer. Since there are three layers, the plate finite element with CLD has 41 DOFs. The DOF vectors can be expressed in the following equations [26,27],

$$\begin{aligned} &\textit{For } i^{th} \textit{ layer } (i = 1,2,3): \\ &\mathbf{U_i} = [u_{mi},\ u_{m(i+1)},\ v_{mi},\ v_{m(i+1)},\ w_m,\ w_1,\ u_{ki},\ u_{k(i+1)},\ v_{ki},\ v_{k(i+1)},\ w_k,\ w_2,\ w_3, \\ &\quad w_4, \\ &\quad u_{pi},\ u_{p(i+1)},\ v_{pi},\ v_{p(i+1)},\ w_p,\ w_5,\ u_{qi},\ u_{q(i+1)},\ v_{qi},\ v_{q(i+1)},\ w_q] \\ &\textit{For three layers}: \\ &\mathbf{U} = [u_{m1},\ u_{m2},\ u_{m3},\ u_{m4},\ v_{m1},\ v_{m2},\ v_{m3},\ v_{m4},\ w_m,\ w_1,\ u_{k1},\ u_{k2},\ u_{k3},\ u_{k4}, \\ &\quad v_{k1},\ v_{k2},\ v_{k3},\ v_{k4},\ w_k,\ w_2,\ w_3,\ w_4,\ u_{p1},\ u_{p2},\ u_{p3},\ u_{p4},\ v_{p1},\ v_{p2},\ v_{p3}, \\ &\quad v_{p4},\ w_p,\ w_5,\ u_{q1},\ u_{q2},\ u_{q3},\ u_{q4},\ v_{q1},\ v_{q2},\ v_{q3},\ v_{q4},\ w_q] \end{aligned} \tag{1}$$

where u_{ji} and $u_{j(i+1)}$ are the longitudinal displacements at the jth point $(j = m, k, p, q)$ of the ith layer along with the x-axis; v_{ji} and $v_{j(i+1)}$ are the longitudinal displacements at the jth point of the ith layer along with the y-axis; and w_n is the transverse displacement at the nth point $(n = m, k, p, q, 1,2,3,4,5)$. Based on the above definition of DOFs, the DOF in the plate structure can be expressed as,

$$n_{DOF} = 9n_x n_y + (3n_x - 2)(n_y - 1) + n_x - 1. \tag{2}$$

Given displacement field, the elastic strain energy and kinetic energy of the ith layer in the plate can be represented as [28–35],

$$V_i = \frac{1}{6}\iiint_{V_i} E_i\left(\left(\frac{\partial u_i}{\partial x}\right)^2 + \frac{\partial u_i}{\partial x}\frac{\partial u_{i+1}}{\partial x} + \left(\frac{\partial u_{i+1}}{\partial x}\right)^2\right) + 3G_i\left(\frac{\partial w_i}{\partial x} - \frac{u_i - u_{i+1}}{2H_i}\right)^2 + 3E_i I_i\frac{\partial^2 w}{\partial x^2} + E_i\left(\left(\frac{\partial v_i}{\partial x}\right)^2 + \frac{\partial v_i}{\partial x}\frac{\partial v_{i+1}}{\partial x} + \left(\frac{\partial v_{i+1}}{\partial x}\right)^2\right) + 3G_i\left(\frac{\partial w_i}{\partial x} - \frac{v_i - v_{i+1}}{2H_i}\right)^2\Bigg)dv, \tag{3}$$

$$T_i = \frac{1}{2}\rho_i\iiint_{V_i}(\dot{u}_i^2 + \dot{v}_i^2 + \dot{w}_i^2)dv, \tag{4}$$

where H_i is the thickness of the ith layer; and G_i are the Young's modulus and shear modulus of the ith layer, respectively; I_i stands for the second moment of area of the plate cross section; and ρ_i is the density of the ith layer.

For the ith layer of the plate finite element, the proposed displacement field can be organized as [30,36–39],

$$\begin{bmatrix} u \\ v \\ w \end{bmatrix} = \mathbf{B}\begin{bmatrix} u_i \\ u_{i+1} \\ v_i \\ v_{i+1} \\ w \end{bmatrix} = \mathbf{B}\begin{bmatrix} F_1 \\ F_2 \\ F_3 \\ F_4 \\ F_5 \end{bmatrix}\mathbf{U_i} = \mathbf{BFU_i} = \mathbf{NU_i} \tag{5}$$

where $\mathbf{B} \in R^{3\times5}$ and $\mathbf{F} \in R^{5\times25}$ are shape function matrices. The matrices $\mathbf{B}$ and $\mathbf{F}$ can be represented as,

$$\mathbf{B_1} = \begin{bmatrix} \frac{z-(H_2+H_3)}{H_1} & 1 - \frac{z-(H_2+H_3)}{H_1} & 0 & 0 & 0 \\ 0 & 0 & \frac{z-(H_2+H_3)}{H_1} & 1 - \frac{z-(H_2+H_3)}{H_1} & 0 \\ 0 & 0 & 0 & 0 & 1 \end{bmatrix} \tag{6}$$

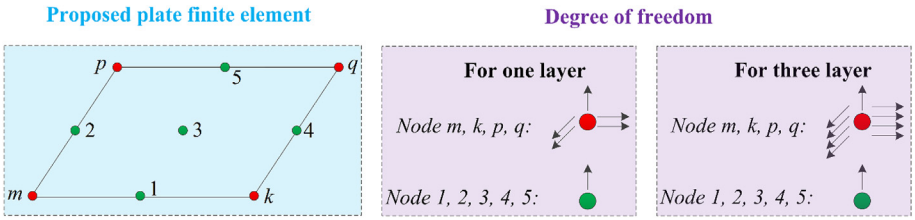

Fig. 2. Proposed plate finite element with analysis of DOF.

Table 1
Simulation parameters.

	Layer 1	Layer 2	Layer 3
Density ($kg{\cdot}m^{-3}$)	2700	1100	2700
Young's modulu (MPa)	6.85×10^4	4.288×10^3	6.65×10^4
Shear modulu (MPa)	2.556×10^4	1.6	2.556×10^4
Thickness (mm)	1	1	1

$$\mathbf{B_2}=\begin{bmatrix} \frac{z-H_3}{H_2} & 1-\frac{z-H_3}{H_2} & 0 & 0 & 0 \\ 0 & 0 & \frac{z-H_3}{H_2} & 1-\frac{z-H_3}{H_2} & 0 \\ 0 & 0 & 0 & 0 & 1 \end{bmatrix} \tag{7}$$

$$\mathbf{B_3}=\begin{bmatrix} \frac{z}{H_3} & 1-\frac{z}{H_3} & 0 & 0 & 0 \\ 0 & 0 & \frac{z}{H_3} & 1-\frac{z}{H_3} & 0 \\ 0 & 0 & 0 & 0 & 1 \end{bmatrix} \tag{8}$$

$$\mathbf{F}=\begin{bmatrix} n_1 & 0 & 0 & 0 & 0 & 0 & n_2 & 0 & 0 & 0 & 0 & 0 & 0 & 0 & n_3 & 0 & 0 & 0 & 0 & 0 & n_4 & 0 & 0 & 0 & 0 \\ 0 & n_1 & 0 & 0 & 0 & 0 & 0 & n_2 & 0 & 0 & 0 & 0 & 0 & 0 & 0 & n_3 & 0 & 0 & 0 & 0 & 0 & n_4 & 0 & 0 & 0 \\ 0 & 0 & n_1 & 0 & 0 & 0 & 0 & 0 & n_2 & 0 & 0 & 0 & 0 & 0 & 0 & 0 & n_3 & 0 & 0 & 0 & 0 & 0 & n_4 & 0 & 0 \\ 0 & 0 & 0 & n_1 & 0 & 0 & 0 & 0 & 0 & n_2 & 0 & 0 & 0 & 0 & 0 & 0 & 0 & n_3 & 0 & 0 & 0 & 0 & 0 & n_4 & 0 \\ 0 & 0 & 0 & 0 & b_1 & b_2 & 0 & 0 & 0 & 0 & b_3 & b_4 & b_5 & b_6 & 0 & 0 & 0 & 0 & b_7 & b_8 & 0 & 0 & 0 & 0 & b_9 \end{bmatrix} \tag{9}$$

where $\mathbf{B}=\mathbf{B_1}$ for the constraining layer; $\mathbf{B}=\mathbf{B}_2$ for the damping layer; $\mathbf{B}=\mathbf{B}_3$ for the base layer; z is the transverse coordinate; n_i and b_i are shape functions; $n_i = y/l_y - xy/l_x l_y$, $n_2 = xy/l_x l_y$, $n_3 = 1 - x/l_x - y/l_y + xy/l_x l_y$, $n_4 = x/l_x - xy/l_x l_y$; x and y are the longitudinal coordinates; l_x and l_y are the length and width of each plate finite element, respectively; $b_1 = l_{1x}l_{3y}$, $b_2 = l_{2x}l_{3y}$, $b_3 = l_{3x}l_{3y}$, $b_4 = l_{1x}l_{2y}$, $b_5 = l_{2x}l_{2y}$, $b_6 = l_{3x}l_{2y}$, $b_7 = l_{1x}l_{1y}$, $b_8 = l_{2x}l_{1y}$, $b_9 = l_{3x}l_{1y}$, $l_{1x} = 2(x-l_x/2)(x-l_x)l_x^2$, $l_{2x} = -4x(x-l_x)l_x^2$, $l_{3x} = 2x(x-l_x/2)l_x^2$, $l_{1y} = 2(y-l_y/2)(y-l_y)l_y^2$, $l_{2y} = -4y(y-l_y)l_y^2$, $l_{3y} = 2y(y-l_y/2)l_y^2$

By substituting Eq. (5) into the elastic strain energy and kinetic energy, the stiffness matrix $\mathbf{KK_i}(\mathbf{KK_i} \in R^{25\times25})$ and mass matrix $\mathbf{MM_i}(\mathbf{MM_i} \in R^{25\times25})$ of the ith layer of the plate finite element can be obtained under certain boundary conditions. Then the stiffness matrix $\mathbf{KK}(\mathbf{KK} \in R^{41\times41})$ and mass matrix $\mathbf{MM}(\mathbf{MM} \in R^{41\times41})$ of the plate finite element can be calculated by Refs. [40–43],

$$\begin{aligned} \mathbf{KK} &= \mathbf{T_1^{-1}KK_1T_1} + \mathbf{T_2^{-1}KK_2T_2} + \mathbf{T_3^{-1}KK_3T_3} \\ \mathbf{MM} &= \mathbf{T_1^{-1}MM_1T_1} + \mathbf{T_2^{-1}MM_2T_2} + \mathbf{T_3^{-1}MM_3T_3} \end{aligned} \tag{10}$$

where $\mathbf{T_i}$ are the matrix with values of 0 and 1, $\mathbf{T_i} \in R^{25\times41}$.

According to the Lagrange formula, the response under a given force vector can be obtained by setting the stiffness matrix and mass matrix [44],

$$\begin{aligned} &\mathbf{M\ddot{X}} + \mathbf{KX} = \mathbf{F} \\ &\mathbf{X} = \mathbf{F}[\mathbf{K} - \omega^2\mathbf{M}]^{-1} \end{aligned} \tag{11}$$

where the response matrix $\mathbf{X} \in R^{n_{DOF}\times1}$ is the DOF vector of the plate with meshed finite elements, which can be obtained by combining the matrix $\mathbf{U}$ in each plate finite element; the stiffness matrix $\mathbf{K} \in R^{n_{DOF}\times n_{DOF}}$ and mass matrix $\mathbf{M} \in R^{n_{DOF}\times n_{DOF}}$ can also be set by integrating the stiffness matrix **KK** and mass matrix **MM** of each finite element in the plate structure; $\mathbf{F} \in R^{n_{DOF}\times n_{DOF}}$ stands for the given force vector; and ω means the inherent frequency of the plate structure.

2.3. Simulation

Based on the proposed FE modeling of the plate structure with CLD, the response characteristics can be obtained by conducting a practical case. The plate is simply supported at two opposite edges. As a result, the transverse displacements at two opposite edges are all zero. The simulation parameters are given in Table 1. A unit force along with the z-axis is excited at the center of the plate structure and three measurement points are selected to calculate their transverse displacements, as shown in Fig. 3 with meshed finite elements. For the plate structure, 9 nodes are used for both longitudinal directions to divide the plate into 64 blocks. For Point 1, its coordinate is (0.2, 0.2). The coordinates are (0.2, 0.3) and (0.2, 0.4) for Points 2 and 3, respectively. Moreover, the response at the excitation point is also calculated. Finally, the result of response is shown in Fig. 4. The result shows that there are always resonances at about 21 Hz, 136 Hz, and 466 Hz. This is caused by the inherent frequency of the plate structure.

3. Simplified single-layer equivalent modeling for plate structures with CLD

This section presents the application of the simplified single-layer equivalent method to model the plate structure with CLD. First, the simplified single-layer equivalent equation involved in the equivalent material properties is defined. Then the equivalent bending stiffness is derived by using nonlinear regression. Based on the equivalent material

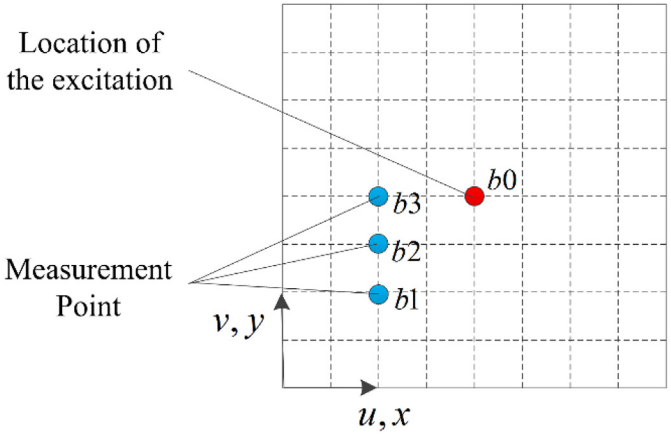

Fig. 3. Plate structure with meshed finite elements.

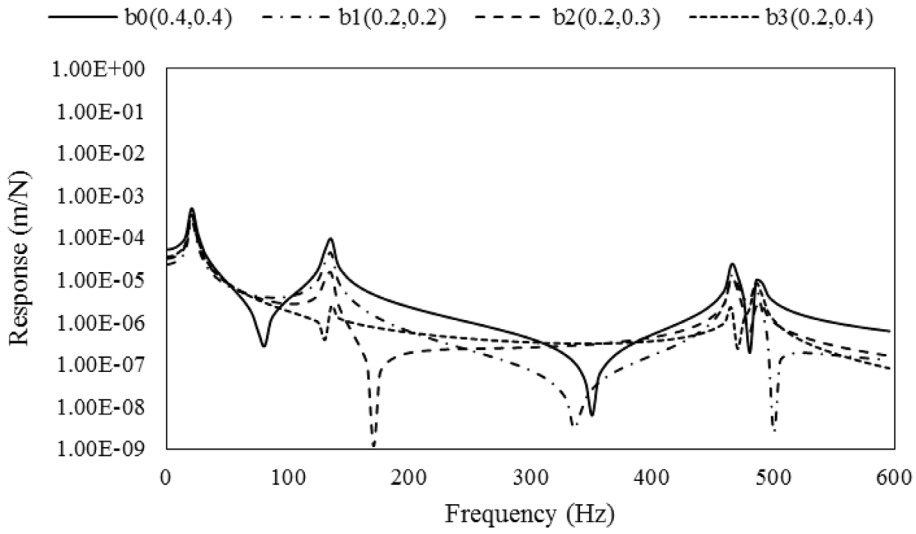

Fig. 4. Responses under finite element modeling of plate structure with CLD.

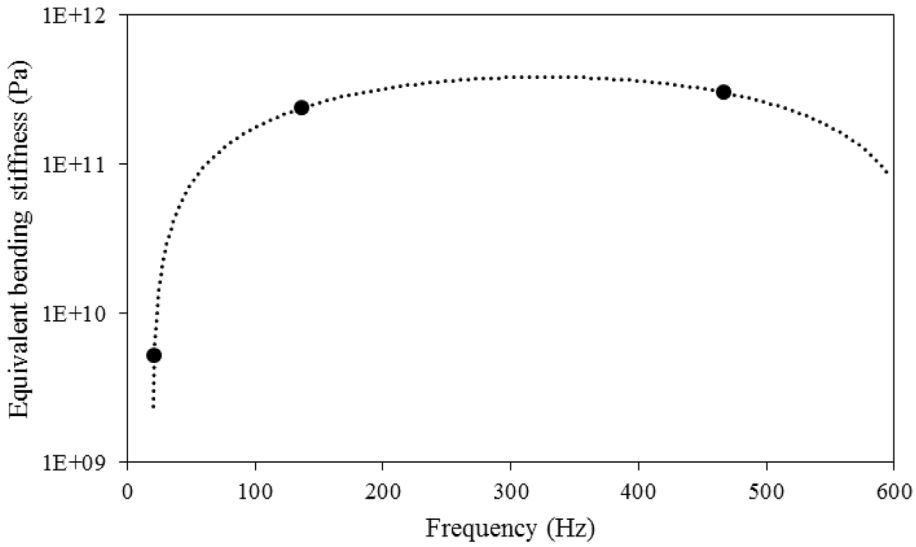

Fig. 5. New approach on calculating equivalent bending stiffness.

properties, a simplified single-layer equivalent model is developed.

3.1. Simplified single-layer equivalent equation

A new equation is defined to calculate the transverse displacement of the plate structure with CLD to reduce the complexity of modeling. The transverse displacement at the measurement point (x, y) can be expressed as [45–50],

$$w(x,y) = \frac{4P_c}{\pi^2 D l l_x l l_y} \sum_{m=1}^{\infty}\sum_{n=1}^{\infty} \frac{\sin\left(\frac{m\pi a}{l l_x}\right)\sin\left(\frac{n\pi b}{l l_y}\right)\sin\left(\frac{m\pi x}{l l_x}\right)\sin\left(\frac{n\pi y}{l l_y}\right)}{\left[\left(\frac{m}{l l_x}\right)^2 + \left(\frac{n}{l l_y}\right)^2\right]^2} \tag{12}$$

where P_c is the point load; ll_x and ll_y are the length and width of the plate structure with CLD; (a, b) represents the location of the loading; D is the flexural rigidity and is defined by,

$$D = \frac{Eh^3}{12(1-\nu^2)} = \frac{Ah^3}{12} \tag{13}$$

where h stands for the thickness of the plate structure with CLD; ν and E represent the equivalent Poisson's ratio and the equivalent Young's modulus of the plate structure with CLD; and A is the equivalent bending stiffness to be found.

In Eq. (12), the superposition of sine function is from m = 1 and n = 1 to infinity, which makes the calculation complex. Therefore, the upper limits of the superposition are set as 1000 in this work.

3.2. Identification of equivalent bending stiffness

As described in Section 2, there are always resonances at some certain frequencies (such as 21 Hz, 136 Hz and 466 Hz in the above simulation). An equivalent bending stiffness is defined in Eq. (13). The equivalent bending stiffness includes the equivalent Poisson's ratio and the equivalent Young's modulus. At three resonance points, the transverse displacements obtained from the proposed FE modeling of the plate structure with CLD can be used to calculate the equivalent bending stiffness via Eq. (12). Then the obtained three values of equivalent bending stiffness can be fitted and connected by using a curve, leading to an equivalent frequency-dependent bending stiffness as shown in Fig. 5. It can be found that the equivalent frequency-dependent bending stiffness almost keeps constant during the middle frequency.

Besides, it should be noted that the equivalent bending stiffness is not a constant value. It varies along with the frequency.

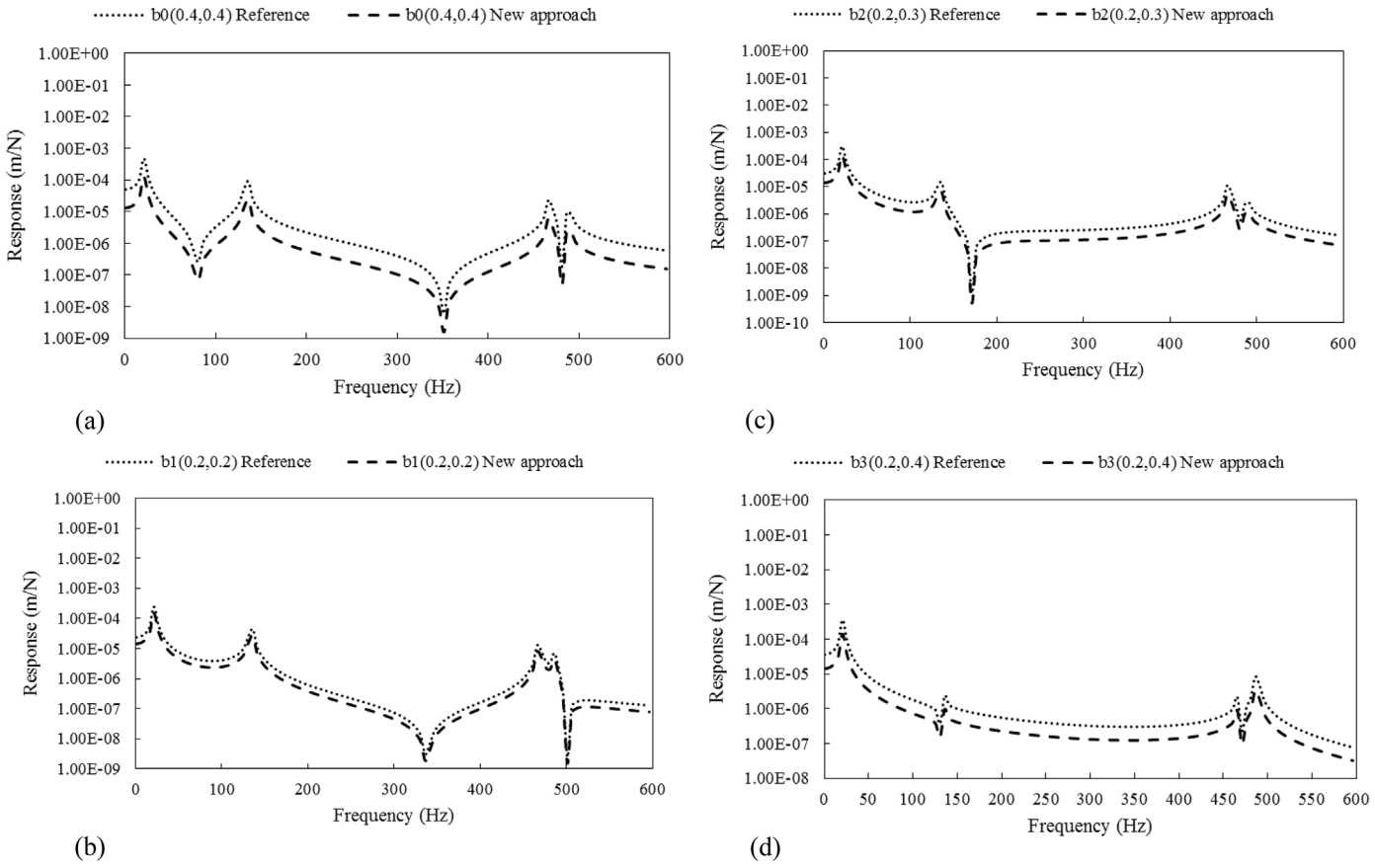

Fig. 6. Comparison of responses at different nodes.

3.3. Simulation results and discussion

Once the equivalent bending stiffness is obtained, the plate structure with CLD can be simplified to a single-layer plate. As a result, a simplified single-layer equivalent modeling can be conducted by using the equivalent material properties, rather than the complex finite element modeling. The same equations for the plate structure with CLD can be used to model simplified single-layer plate with less DOFs, simple structure and low computational cost. Specifically, the DOF decreases from 41 to 25. Based on the plate finite element with 25 DOFs and equivalent bending stiffness, the simplified finite element modeling for plates with CLD can be conducted by using the corresponding stiffness matrix and mass matrix in one layer.

To illustrate the accuracy of the simplified single-layer equivalent model in dealing with the plate structures with CLD, a simulation is carried out for the same plate used in Section 2. The responses under simplified single-layer equivalent model and finite element model are shown in Fig. 6. From these results, it can be found that they have the same resonance frequencies at each node. Furthermore, the responses are almost consistent at the same frequency. In addition, the errors of the responses between the proposed method and the finite element method are different. Specifically, the maximum error appears at the location of the excitation point b0, while the minimum error appears at the location of the measurement point b1. This reflects that a higher accuracy for responses exists at the location far away from the excitation point when the plate structure with CLD is modelled by the proposed method. Therefore, the proposed simplified single layer equivalent method is efficient and accurate for modeling the plate structures with CLD.

In summary, the simplified single-layer equivalent method provides an efficient and fast approach for modeling the complex plate structures with CLD.

4. Conclusions

This paper proposes a new simplified single-layer equivalent method to model the plate structure with CLD based on equivalent material properties. First, the finite element modeling of the plate structure with CLD is carried out, which provides a reference for the proposed method. Then a new equation is defined to derive the equivalent bending stiffness. With the equivalent bending stiffness, a simplified single-layer is constructed to simplify the finite element modeling. The numerical simulation shows that the proposed simplified single-layer equivalent method using single-layer equivalent material properties is efficient and accurate. In addition, the proposed method can give guidance in the model development stage for the active vibration control of high-performance lightweight smart structures, such as wind turbine, helicopter and aircraft structures and so on. In the future, the plates with different boundary conditions and loading modes should be studies. Besides, experiments can be carried out to verify the proposed finite element modeling method and simplified single-layer equivalent method for plate structures with CLD.

Acknowledgements

This work is supported by the Science and Technology Development Fund of Macau S.A.R (Grant No. 012/2015/A), Research Grant of the University of Macau (Grant numbers: MYRG2016-00212-FST and MYRG2017-00135-FST), and the National Natural Science Foundation of China (Grant Numbers: 51705084 and 51878184).

Appendix A. Supplementary data

Supplementary data related to this article can be found at https://doi.org/10.1016/j.compositesb.2018.09.010.

References

[1] Madeira JFA, Araujo AL, Soares CMM. Multiobjective optimization of constrained layer damping treatments in composite plate structures. Mech Compos Mater Struct 2017;24:427–36.

[2] Xu J, Jia Y, Liu B, Zhao H, Yu H, Li J, et al. Coupling effect of state-of-health and state-of-charge on the mechanical integrity of lithium-ion batteries. Exp Mech 2018;58:633–43.

[3] Zhao J, Wong PK, Ma X, Xie Z. Chassis integrated control for active suspension, active front steering and direct yaw moment systems using hierarchical strategy. Veh Syst Dyn 2017;55:72–103.

[4] Ma X, Wong PK, Zhao J. Cornering stability control for vehicles with active front steering system using T-S fuzzy based sliding mode control strategy. Mech Syst Signal Process 2018https://doi.org/10.1016/j.ymssp.2018.05.059.

[5] Zhao J, Wong PK, Ma X, Xie Z. Design and analysis of an integrated SMC-TPWP strategy for a semi-active air suspension with stepper motor-driven GFASA. Proc IME J Syst Contr Eng 2018https://doi.org/10.1177/0959651818778217.

[6] Ma X, Wong PK, Zhao J. Practical multi-objective control for automotive semi-active suspension system with nonlinear hydraulic adjustable damper. Mech Syst Signal Process 2019;117:667–88.

[7] Zhao J, Wong PK, Xie Z, Ma X, Hua X. Design and control of an automotive variable hydraulic damper using cuckoo search optimized PID method. Int J Automot Technol 2018. in press.

[8] Zhao J, Wong PK, Xie ZC, Ma XB. Cuckoo search-based intelligent control of a novel variable rotary valve system for engines using PID controller. J Intell Fuzzy Syst 2017;32:2351–63.

[9] Roozen NB, Labelle L, Leclère Q, Ege K, Alvarado S. Non-contact experimental assessment of apparent dynamic stiffness of constrained-layer damping sandwich plates in a broad frequency range using a Nd:YAG pump laser and a laser Doppler vibrometer. J Sound Vib 2017;395:90–101.

[10] Xu J, Wu Y, Wang L, Li J, Yang Y, Tian Y, et al. Compressive properties of hollow lattice truss reinforced honeycombs (Honeytubes) by additive manufacturing: patterning and tube alignment effects. Mater Des 2018;156:446–57.

[11] Xu J, Wu Y, Gao X, Wu H, Steven N, Yin S. Design of composite lattice materials combined with fabrication approaches. J Compos Mater 2018https://doi.org/10.1177/0021998318785710.

[12] Ma X, Wong PK, Zhao J. Adaptive regulating of automotive mono-tube hydraulic adjustable dampers using grey neural network-based compensation system. Proc Inst Mech Eng - Part D J Automob Eng 2018. in press.

[13] Wang Y, Khanoki SA, Tanzer M, Pasini D. Hip implant design with three-dimensional porous architecture of optimized graded density. J Mech Des 2018. https://doi.org/10.1115/1.4041208.

[14] Wang Y, Xu H, Pasini D. Multiscale isogeometric topology optimization for lattice materials. Comput Meth Appl Mech Eng 2017;316:568–85.

[15] Panda RK, Nayak B, Sarangi SK. Active vibration control of smart functionally graded beams. Proc Eng 2016;144:551–9.

[16] Ozer AO. Modeling and controlling an active constrained layer (ACL) beam actuated by two voltage sources with/without magnetic effects. IEEE Trans Automat Contr 2017;64:6445–50.

[17] Hujare PP, Sahasrabudhe AD. Experimental investigation of damping performance of viscoelastic material using constrained layer damping treatment. Proc Mater Sci 2014;5:726–33.

[18] Castel A, Loredo A, Hafidi AE, Martin B. Complex power distribution analysis in plates covered with passive constrained layer damping patches. J Sound Vib 2012;331:2485–98.

[19] Wong PK, Xie ZC, Zhao J, Xu T, He F. Analysis of automotive rolling lobe air spring under alternative factors with finite element model. J Mech Sci Technol 2014;28:5069–81.

[20] Xie Z, Steve Shepard W. Development of a single-layer finite element and a simplified finite element modeling approach for constrained layer damped structures. Finite Elem Anal Des 2009;45:530–7.

[21] Xie Z, Wong PK, Zhang L, Wong HC. Numerical modeling and control of rotating plate with coupled self-sensing and frequency-dependent active constrained layer damping. Math Probl Eng 2012:939–55. 2012.

[22] Shi Z, Yao X, Pang F, Wang Q. A semi-analytical solution for in-plane free vibration analysis of functionally graded carbon nanotube reinforced composite circular arches with elastic restraints. Compos Struct 2017;182:420–34.

[23] Yin S, Chen H, Wu Y, Li Y, Xu J. Introducing composite lattice core sandwich structure as an alternative proposal for engine hood. Compos Struct 2018;201:131–40.

[24] Hu J, Yin S, Yu TX, Xu J. Dynamic compressive behavior of woven flax-epoxy-laminated composites. Int J Impact Eng 2018;117:63–74.

[25] Zapfe JA, Lesieutre GA. A discrete layer beam finite element for the dynamic analysis of composite sandwich beams with integral damping layers. Comput Struct 1999;70:647–66.

[26] Zhao J, Choe K, Xie F, Wang A, Shuai C, Wang Q. Three-dimensional exact solution for vibration analysis of thick functionally graded porous (FGP) rectangular plates with arbitrary boundary conditions. Compos B Eng 2018. https://doi.org/10.1016/j.compositesb.2018.09.001.

[27] Zhao J, Choe K, Xie F, Wang A, Shuai C, Wang Q. Free vibration analysis of laminated composite elliptic cylinders with general boundary conditions. Compos B Eng 2018. in press.

[28] Choe K, Tang J, Shui C, Wang A, Wang Q. Free vibration analysis of coupled functionally graded (FG) doubly-curved revolution shell structures with general boundary conditions. Compos Struct 2018;194:413–32.

[29] Choe K, Wang Q, Tang J, Shui C. Vibration analysis for coupled composite laminated axis-symmetric doubly-curved revolution shell structures by unified Jacobi-Ritz Method. Compos Struct 2018;194:136–57.

[30] Guan X, Tang J, Shi D, Shuai C, Wang Q. A semi-analytical method for transverse vibration of sector-like thin plate with simply supported radial edges. Appl Math Model 2018;60:48–63.

[31] Guan X, Tang J, Wang Q, Shuai C. Application of the differential quadrature finite element method to free vibration of elastically restrained plate with irregular geometries. Eng Anal Bound Elem 2018;90:1–16.

[32] Guo J, Shi D, Wang Q, Pang F, Liang Q. A domain decomposition approach for static and dynamic analysis of composite laminated curved beam with general elastic restrains. Mech Adv Mater Struct 2018:1–13.

[33] Zhong R, Wang Q, Tang J, Shuai C, Qin B. Vibration analysis of functionally graded carbon nanotube reinforced composites (FG-CNTRC) circular, annular and sector plates. Compos Struct 2018;194:49–67.

[34] Zhao J, Xie F, Wang A, Shuai C, Tang J, Wang Q. Vibration behavior of the functionally graded porous (FGP) doubly-curved panels and shells of revolution by using a semi-analytical method. Compos B Eng 2018;157:219–38.

[35] Zhang H, Shi D, Wang Q, Zha S. Vibro-acoustic analysis of the annular segment flexible plate coupled with an impedance walled enclosure. Thin-Walled Struct 2018;131:205–22.

[36] Xie Z, Xue X. A new plate finite element model for rotating plate structures with constrained damping layer. Finite Elem Anal Des 2011;47:487–95.

[37] Zhang H, Shi D, Zha S, Wang Q. Parameterization study on the moderately thick laminated rectangular plate-cavity coupling system with uniform or non-uniform boundary conditions. Compos Struct 2018;194.

[38] Zhang H, Shi D, Zha S, Wang Q. A simple first-order shear deformation theory for vibro-acoustic analysis of the laminated rectangular fluid-structure coupling system. Compos Struct 2018;201:647–63.

[39] Zhou Y, Wang Q, Shi D, Liang Q, Zhang Z. Exact solutions for the free in-plane vibrations of rectangular plates with arbitrary boundary conditions. Int J Mech Sci 2017;130:1–10.

[40] Wang Q, Pang F, Qin B, Liang Q. A unified formulation for free vibration of functionally graded carbon nanotube reinforced composite spherical panels and shells of revolution with general elastic restraints by means of the Rayleigh–Ritz method. Polym Compos 2017;39:E924–44.

[41] Wang Q, Qin B, Shi D, Liang Q. A semi-analytical method for vibration analysis of functionally graded carbon nanotube reinforced composite doubly-curved panels and shells of revolution. Compos Struct 2017;174:87–109.

[42] Wang Q, Shao D, Qin B. A simple first-order shear deformation shell theory for vibration analysis of composite laminated open cylindrical shells with general boundary conditions. Compos Struct 2017;184:211–32.

[43] Xiao Y, Shao D, Zhang H, Shuai C, Wang Q. An acoustic modeling of the three-dimensional annular segment cavity with various impedance boundary conditions. Result Phys 2018;10:411–23.

[44] Xie Z, Shepard WS, Woodbury KA. Design optimization for vibration reduction of viscoelastic damped structures using genetic algorithms. Shock Vib 2013;16:455–66.

[45] Zhao J, Xie F, Wang A, Shuai C, Tang J, Wang Q. A unified solution for the vibration analysis of functionally graded porous (FGP) shallow shells with general boundary conditions. Compos B Eng 2018https://doi.org/10.1016/j.compositesb.2018.08.115.

[46] Zhao J, Xie F, Wang A, Shuai C, Tang J, Wang Q. Dynamics analysis of functionally graded porous (FGP) circular, annular and sector plates with general elastic restraints. Compos B Eng 2018https://doi.org/10.1016/j.compositesb.2018.08.114.

[47] Wang Q, Choe K, Shi D, Sin K. Vibration analysis of the coupled doubly-curved revolution shell structures by using Jacobi-Ritz Method. Int J Mech Sci 2018;135:517–31.

[48] Wang Q, Cui X, Qin B, Liang Q. Vibration analysis of the functionally graded carbon nanotube reinforced composite shallow shells with arbitrary boundary conditions. Compos Struct 2017;182:364–79.

[49] Guo J, Shi D, Wang Q, Tang J, Shuai C. Dynamic analysis of laminated doubly-curved shells with general boundary conditions by means of a domain decomposition method. Int J Mech Sci 2018;138:159–86.

[50] Wang Q, Cui X, Qin B, Liang Q, Tang J. A semi-analytical method for vibration analysis of functionally graded (FG) sandwich doubly-curved panels and shells of revolution. Int J Mech Sci 2017;134:479–99.